

NACA RM A54DO5

UNCLASSIFIED



RESEARCH MEMORANDUM

WIND-TUNNEL INVESTIGATION AT SUBSONIC AND SUPERSONIC SPEEDS
OF A FIGHTER MODEL EMPLOYING A LOW-ASPECT-RATIO UNSWEPT
WING AND A HORIZONTAL TAIL MOUNTED WELL ABOVE THE
WING PLANE - LONGITUDINAL STABILITY AND CONTROL

By Willard G. Smith

Ames Aeronautical Laboratory
Moffett Field, Calif.

LANGLEY AERONAUTICAL LABORATORY
LIBRARY 2213
LANGLEY FIELD, VIRGINIA

CLASSIFICATION CHANGED

To UNCLASSIFIED

By authority of HPA # 17 effective 3/18/60
CLASSIFIED DOCUMENT

This material contains information affecting the National Defense of the United States within the meaning of the espionage laws, Title 18, U.S.C., Secs. 793 and 794, the transmission or revelation of which in any manner to an unauthorized person is prohibited by law.

NATIONAL ADVISORY COMMITTEE FOR AERONAUTICS

WASHINGTON

November 15, 1954

UNCLASSIFIED

[REDACTED]
NATIONAL ADVISORY COMMITTEE FOR AERONAUTICSRESEARCH MEMORANDUMWIND-TUNNEL INVESTIGATION AT SUBSONIC AND SUPERSONIC SPEEDS
OF A FIGHTER MODEL EMPLOYING A LOW-ASPECT-RATIO UNSWEPT
WING AND A HORIZONTAL TAIL MOUNTED WELL ABOVE THE
WING PLANE - LONGITUDINAL STABILITY AND CONTROL

By Willard G. Smith

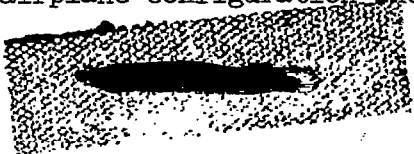
SUMMARY

Experimental results showing the static longitudinal-stability and -control characteristics of a model of a fighter airplane employing a low-aspect-ratio unswept wing and an all-movable horizontal tail are presented. The investigation was made over a Mach number range from 0.60 to 0.90 and from 1.35 to 1.90 at a constant Reynolds number of 2.40 million, based on the wing mean aerodynamic chord.

The pitching moments of the model as influenced by the horizontal-tail location are of particular interest. The influence of the vertical-tail pressure field in inducing a horizontal tail load which gives a positive pitching moment at zero lift and of the wing downwash on the longitudinal stability is discussed and the effect on trim drag noted. Information pertaining to the effectiveness of the all-movable horizontal tail as a control surface is also given.

INTRODUCTION

The characteristics of aircraft configurations capable of supersonic flight have received considerable attention during the past several years. One of the problems associated with the low-aspect-ratio wings employed on these high-speed airplanes is the wing-tail interference, especially in the landing attitude. Investigation of the effects of tail height on configurations with sweptback or triangular wings (refs. 1 to 8) have shown that a high tail position produces undesirable longitudinal-stability changes at high angles of attack as the tail passes through the vortex field from the wing. An airplane configuration incorporating a thin,



low-aspect-ratio, unswept wing and a high horizontal-tail position has recently been investigated in the Ames 6- by 6-foot supersonic wind tunnel. In view of the deficiency of the high tail position on aircraft with sweptback and triangular wings and the paucity of information concerning the effect of tail position on aircraft with unswept wings, it was thought that the data obtained during the present investigation concerning the longitudinal-stability characteristics would be of considerable general interest. This report presents, therefore, the longitudinal-stability and -control characteristics of this supersonic airplane configuration.

NOTATION

b wing span, in.

c local wing chord measured parallel to model plane of symmetry, in.

\bar{c} wing mean aerodynamic chord, $\frac{\int_0^{b/2} c^2 dy}{\int_0^{b/2} c dy}$, in.

C_D drag coefficient, $\frac{\text{drag}}{qS}$

C_L lift coefficient, $\frac{\text{lift}}{qS}$

$C_{L\delta}$ rate of change of lift coefficient with horizontal-tail deflection measured at zero deflection angle, per deg

C_m pitching-moment coefficient, referred to the quarter point of the mean aerodynamic chord of the wing, $\frac{\text{pitching moment}}{qS\bar{c}}$

$C_{m\delta}$ rate of change of pitching-moment coefficient with horizontal-tail deflection measured at zero deflection angle, per deg

$\frac{dC_m}{dC_L}$ rate of change of pitching-moment coefficient with lift coefficient measured at zero lift

$\frac{L}{D}$ lift-drag ratio

- M free-stream Mach number
- q free-stream dynamic pressure, lb/sq in.
- S total wing area measured in the plane of each wing panel and including the area formed by extending the leading and trailing edges to the model plane of symmetry, sq in.
- y spanwise distance from plane of symmetry, in.
- α angle of attack of fuselage longitudinal axis, deg
- δ angle of deflection of horizontal tail measured with respect to the fuselage reference axis, deg
- ϵ downwash angle, deg

APPARATUS

The Ames 6- by 6-foot supersonic wind tunnel is a variable-pressure wind tunnel in which Mach number can be changed continuously from 0.60 to 0.90 and from 1.20 to 1.90. Further information pertaining to this wind tunnel and characteristics of the air stream are given in reference 9. In the wind tunnel, models are mounted on a sting support system in which the plane of motion is horizontal in order to utilize the most favorable stream conditions in the test section. During the present investigation, a 2.5-inch, six-component, strain-gage balance mounted in the fuselage of the model was used to measure the aerodynamic forces and moments.

As shown in the photograph of figure 1 and the sketch of figure 2, the model used in the present investigation consisted of a wing, fuselage, and tail. The wing was attached to the model so as to permit the dihedral angle to be changed. For the major portion of the investigation the dihedral angle was -5° . An angle of -10° was also used for a small portion of the investigation. The fuselage was basically a body of revolution to which were added a canopy and fairings at the wing roots to simulate the protuberances associated with the side inlets. The tail assembly shown in figures 1 and 2 was used during the major portion of the investigation and, for brevity, will be referred to as the "standard tail." The horizontal surface of the standard tail could be mounted at several different deflection angles in order to measure the effectiveness of the surface. Two other tail assemblies were also investigated and their shapes are compared with the standard tail assembly in figure 3. The horizontal surface was the same for all tail assemblies. During the investigations of the low-tail configuration only, the dihedral of the wing was -10° .

The wing and tail assemblies were machined from solid steel. The fuselage was machined from aluminum.

Dimensions of the model are given in figure 2. Other pertinent geometric characteristics of the model are presented in the following table:

Wing

Section	elliptical forward of 50-percent chord and biconvex aft	
Thickness, percent		3.4
Area, sq in.		202.46
Aspect ratio		2.5
Taper ratio		0.385
Sweep of leading edge		27° 7'

Horizontal tail

Section	elliptical forward of 50-percent chord and biconvex aft	
Root thickness, percent		5
Tip thickness, percent		3
Area, sq in.		49.80
Aspect ratio		2.889
Taper ratio		0.326
Distance from $\bar{c}/4$ of wing to $\bar{c}/4$ of tail, in.		17.22

REDUCTION OF DATA

The forces and moments measured by the strain-gage balance have been resolved into standard NACA coefficient form as defined in the Notation section presented herein. The forces and moments are presented with respect to the wind axes with the origin on the fuselage center line at the lateral projection of the quarter point of the mean aerodynamic chord of the wing. Certain corrections have been made to the data to account for differences known to exist between measurements made in a wind tunnel and in free air. These corrections account for the following factors:

1. The longitudinal force on the model resulting from a static-pressure gradient in the test section as determined from a tunnel-empty calibration
2. The increase in airspeed in the vicinity of the model at subsonic speeds resulting from constriction effects of the tunnel walls
3. The change in angle of attack in the vicinity of the model induced by the tunnel walls at subsonic speeds as a result of the lift on the model

In addition to the aforementioned corrections, the drag data were also adjusted to correspond to conditions in which the pressure at the base of the model would be free-stream static pressure. This adjustment partially accounts for the effects of sting interference. No further corrections were made for the effects of sting interference. Tests were made using a sting with a constant diameter, extending approximately four diameters aft of the model base, to evaluate the influence of the tapered sting used for this investigation on the aerodynamic characteristics of the model. Results of these tests on the model with the low horizontal-tail position indicate that the tapered sting, at subsonic speeds, produced a reduction in measured drag of about 0.0010 and a negative shift in the pitching-moment curve equivalent to one-third of a degree horizontal-tail deflection. However, the slopes of the pitching-moment curves and the control effectiveness were essentially unaffected by the influence of the sting. At supersonic speeds the sting influence was negligible.

RESULTS AND DISCUSSION

The results of the present investigation revealed several interesting phenomena concerning the pitching-moment coefficient at zero lift and the longitudinal-stability characteristics of the model. These effects are believed to be associated with the high position of the horizontal tail on the model and will be discussed in some detail in the first portion of this section of the report. Following this discussion, the control characteristics will be presented, including the control effectiveness and the drag coefficient of the complete model for a condition of balance.

The Pitching Moment at Zero Lift

The results in figure 4 and, in particular, figure 5, show that throughout the Mach number range of this investigation, the pitching-moment coefficient at zero lift for the model either without the horizontal tail or with any of the horizontal tails at zero deflection was positive. If the influence of the tapered sting had been considered, the value of pitching-moment coefficient for the model with any of the horizontal tails would have been more positive. For the model without a horizontal tail, the positive value of pitching moment was small and was probably caused by the asymmetrical drag forces of the canopy and vertical tail. More significant, however, was the large positive value of pitching moment contributed by any of the horizontal tails at zero deflection, particularly at moderate supersonic speeds (see fig. 5). The lift characteristics of the model (fig. 4) show that the positive increment of pitching-moment coefficient attributable to the horizontal tail was produced by a negative lift on the horizontal tail. The negative lift is believed to be caused by the pressure field induced by the profile of the vertical tail reducing

the pressure on the lower surface of the horizontal tail only, since this surface is located at the tip of the vertical tail. To verify this reasoning, a calculation was made for a Mach number of 1.35 wherein it was assumed that the pressure distribution at the surface of the vertical tail (measured experimentally for a similar section) was projected laterally along Mach lines; this pressure field could be superimposed on the pressure distribution of that portion of the lower surface of the horizontal tail lying within the Mach lines from the leading and trailing edges of the vertical tail. These calculated results accounted for approximately 90 percent of the pitching-moment coefficient at zero lift. Also in agreement with this reasoning are the effects of horizontal-tail position and increase in Mach number on the pitching-moment coefficient at zero lift, as determined experimentally during the present investigation. The results of figure 5 show that a forward movement of the horizontal tail or an increase in supersonic Mach number reduced the pitching-moment coefficient at zero lift. Both effects can be accounted for by the fact that the portion of the lower surface of the horizontal tail lying within the Mach lines from the leading and trailing edges of the vertical tail was reduced.

Longitudinal Stability

The pitching-moment characteristics at lift coefficient in the subsonic speed range show that the stability of the model either with or without a horizontal tail was considerably greater at lift coefficients above 0.50 than at lower lift coefficients. The change of stability with lift coefficient was most pronounced for the model without a horizontal tail at a Mach number of 0.80; for all subsonic Mach numbers the effect was less for the model with than without the horizontal tails. The latter characteristic was due to a reduction in the stability contribution of the horizontal tail at higher lift coefficients caused by an increase in the rate of change of downwash angle with angle of attack. The effective downwash angle, as determined from the model with the standard tail at several deflection angles, is shown in figure 6. The data for subsonic speeds indicate that the value of $d\epsilon/d\alpha$ at angles of attack above 8° was twice as great as that at 0° . Thus, in a manner similar to that for triangular and sweptback wings, the stability contribution of the high horizontal tail decreased considerably with increasing angle of attack as the tail passed through the vortex field from the wing. In the present case, these effects were favorable in that they reduced the excessive stability changes with increasing lift coefficient shown by the model without a horizontal tail.

Further effects of the wing on the horizontal-tail load are indicated by the stability characteristics of the model at Mach numbers of 1.45 and above. At a supersonic Mach number of 1.35, the longitudinal stability of the model with any of the three horizontal tails was essentially constant throughout the lift-coefficient range of the tests. With increase

in Mach number above 1.35 for the model with the forward-tail configuration and above 1.60 for the model with either the standard- or low-tail configuration, the stability near zero lift reduced (see fig. 7); whereas that at the high lift coefficients remained approximately the same as at the lower supersonic Mach number. Furthermore, the lift-coefficient range for reduced stability increased with Mach number. The phenomenon was most pronounced for the forward-tail configuration and was sufficiently effective, so that the slope of the pitching-moment curve (fig. 4) at a Mach number of 1.90 was almost identical to the slopes in the subsonic range of the investigation up to a lift coefficient of approximately 0.60. This reduction in the stability contribution of the horizontal tail at high supersonic Mach numbers and low lift coefficients was due to an increase in the value of $d\epsilon/d\alpha$, as shown for the standard-tail configuration in figure 6.

The increase in the parameter $d\epsilon/d\alpha$ at low lift coefficients can be explained by the fact that with increasing Mach number, the inclination of the shock wave at the wing trailing edge increased so that, eventually, the horizontal tail was ahead of the shock wave. The stream angle ahead of the shock wave was nearly equal to the angle of attack of the wing. Thus, as Mach number increased, the shock wave passed by the horizontal tail and the rate of change of effective downwash at the horizontal tail with angle of attack increased. With increasing angle of attack at a constant Mach number, the horizontal tail moved below the shock wave and into a flow field where $d\epsilon/d\alpha$ was small. It is evident from this description of the cause of the phenomenon at supersonic speeds why the reduced stability region for the forward-tail configuration was observed at a lower Mach number and why it extended over a wider range of lift coefficients than for either the standard- or low-tail configurations. It also can be seen that the range of lift coefficients for reduced stability will increase with Mach number.

The results of figure 4 also show that the model with any of the tail configurations and having the center of gravity at the quarter point of the wing mean aerodynamic chord was stable throughout the range of the investigation. Excluding the lift-coefficient range near the stall, a minimum static margin of 5 percent was obtained at the subsonic Mach numbers between lift coefficients of approximately 0.2 and 0.4.

Longitudinal Control

The longitudinal-control characteristics were determined during the present investigation for the standard-tail configuration only. Furthermore, at Mach numbers of 0.60 and 1.80, data were obtained at a horizontal-tail deflection of 0° only; whereas at the remaining Mach numbers, data were also obtained at deflections of $+4^\circ$ and -8° . The results of figure 4 show that throughout the lift-coefficient range of the investigation, the

lift and pitching-moment effectiveness of the horizontal tail remained essentially constant at all the test Mach numbers except Mach number 1.90, where the control effectiveness decreased slightly with increasing angle of attack. This decrease is probably the result of a dynamic pressure loss at the horizontal tail as it moves down through the shock wave from the wing trailing edge with increasing angle of attack. The results of figure 8, showing the effectiveness parameters $C_{L\delta}$ and $C_{m\delta}$ are, therefore, applicable throughout the lift-coefficient range, except at a Mach number of 1.90. Also shown in figure 8 are estimates of the effectiveness parameters using the methods of reference 10 for subsonic Mach numbers and those of reference 11 for supersonic Mach numbers. The estimated results show the same general trends as the experimental results, although differing in value by as much as 12 percent.

The lift coefficient, drag coefficient, and tail deflections for balance are shown in figure 9. The aforementioned increase in stability above a lift coefficient of 0.50 in the subsonic speed range is reflected in these data by an increase in the rate of change of deflection angle with lift coefficient. The influence of the wing on the tail at low lift coefficients at a Mach number of 1.90 and the effect of the vertical-tail pressure field on the horizontal-tail load are evident in the deflection angle of the all-movable horizontal tail required for balance. A comparison of the trim drag with the drag for the model without a horizontal tail (fig. 4) shows that in the balanced condition at supersonic speeds, the drag attributable to the horizontal tail between lift coefficients of 0.2 and 0.4 is less than 12 percent of the total drag. The small penalty of drag for trim is a result of the favorable influence of the vertical tail on the horizontal tail which reduces the control deflections required for trim.

CONCLUDING REMARKS

A study of the results of the investigation shows:

1. The trim drag of the model is reduced by the favorable influence of the flow field due to thickness of the vertical tail on the pitching moment at zero lift.
2. No serious adverse effects of the wing flow field on the pitching moment due to the horizontal tail were noted. The influence on airplane flying qualities of the impingement of the trailing-edge shock wave of the wing on the horizontal tail is not known, however.

Ames Aeronautical Laboratory
National Advisory Committee for Aeronautics
Moffett Field, Calif., Apr. 5, 1954

REFERENCES

1. Allen, Edwin C.: Investigation of a Triangular Wing in Conjunction with a Fuselage and Horizontal Tail to Determine Downwash and Longitudinal-Stability Characteristics - Transonic Bump Method. NACA RM A51F12a, 1951.
2. Graham, David, and Koenig, David G.: Tests in the Ames 40- by 80-Foot Wind Tunnel of an Airplane Configuration with an Aspect Ratio 2 Triangular Wing and an All-Movable Horizontal Tail - Longitudinal Characteristics. NACA RM A51B21, 1951.
3. Jaquet, Byron M.: Effects of Horizontal-Tail Position, Area, and Aspect Ratio on Low-Speed Static Longitudinal Stability and Control Characteristics of a 60° Triangular-Wing Model Having Various Triangular-All-Movable Horizontal Tails. NACA RM L51I06, 1951.
4. Foster, Gerald V., and Griner, Roland F.: Low-Speed Longitudinal and Wake Air-Flow Characteristics at a Reynolds Number of 5.5×10^6 of a Circular-Arc 52° Sweptback Wing With a Fuselage and a Horizontal Tail at Various Vertical Positions. NACA RM L51C30, 1951.
5. Purser, Paul E., Spearman, M. Leroy, and Bates, William R.: Preliminary Investigation at Low Speed of Downwash Characteristics of Small-Scale Sweptback Wings. NACA TN 1378, 1947.
6. Myers, Boyd C., II, and King, Thomas J., Jr.: Aerodynamic Characteristics of a Wing with Quarter-Chord Line Swept Back 45°, Aspect Ratio 4, Taper Ratio 0.3, and NACA 65A006 Airfoil Section. Transonic-Bump Method. NACA RM L9E25, 1949.
7. Myers, Boyd C., II, and King, Thomas J., Jr.: Aerodynamic Characteristics of a Wing with Quarter-Chord Line Swept Back 60°, Aspect Ratio 2, Taper Ratio 0.6, and NACA 65A006 Airfoil Section. Transonic-Bump Method. NACA RM L50A12, 1950.
8. King, Thomas J., Jr., and Myers, Boyd C., II: Aerodynamic Characteristics of a Wing with Quarter-Chord Line Swept Back 60°, Aspect Ratio 4, Taper Ratio 0.6, and NACA 65A006 Airfoil Section. NACA RM L9G27, 1949.
9. Frick, Charles W., and Olson, Robert N.: Flow Studies in the Asymmetric Adjustable Nozzle of the Ames 6- by 6-Foot Supersonic Wind Tunnel. NACA RM A9E24, 1949.
10. DeYoung, John, and Harper, Charles W.: Theoretical Symmetric Span Loading at Subsonic Speeds for Wings Having Arbitrary Plan Form. NACA Rep. 921, 1948.

11. Lapin, Ellis: Charts for the Computation of Lift and Drag of Finite Wings at Supersonic Speeds. Douglas Aircraft Co. Rep. SM-13480, Oct. 1949.

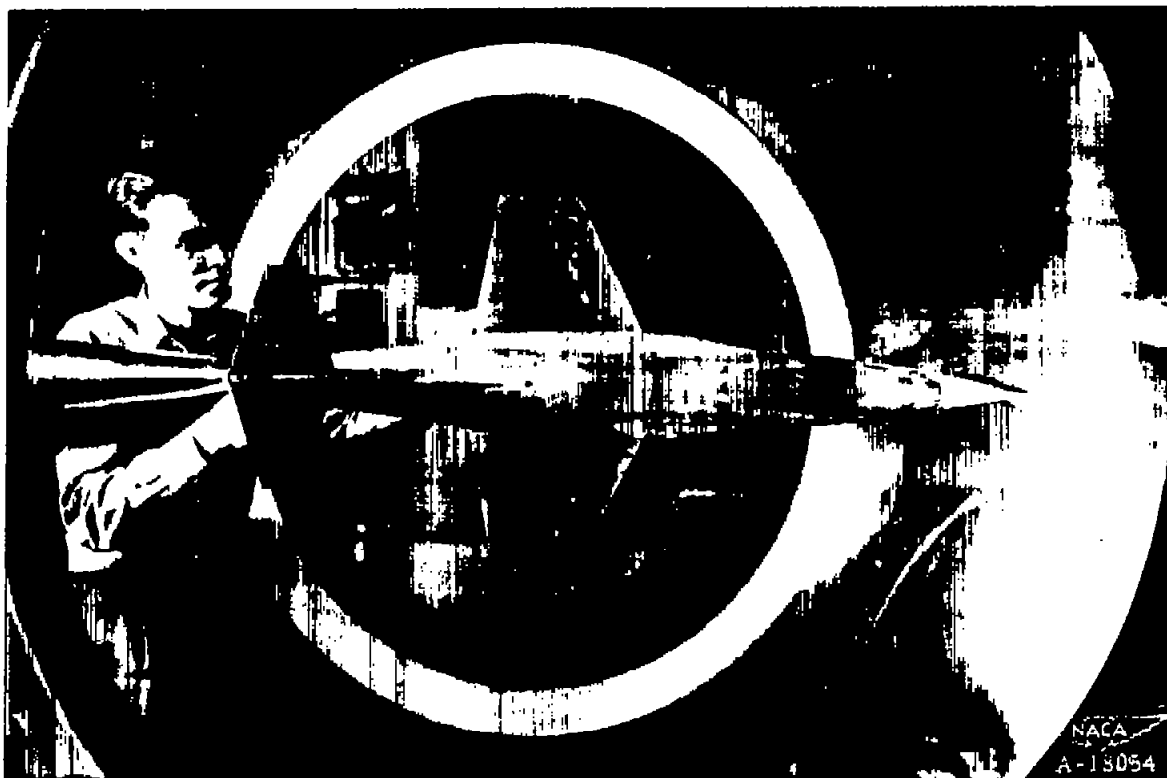


Figure 1.- Photograph of the model in the tunnel.

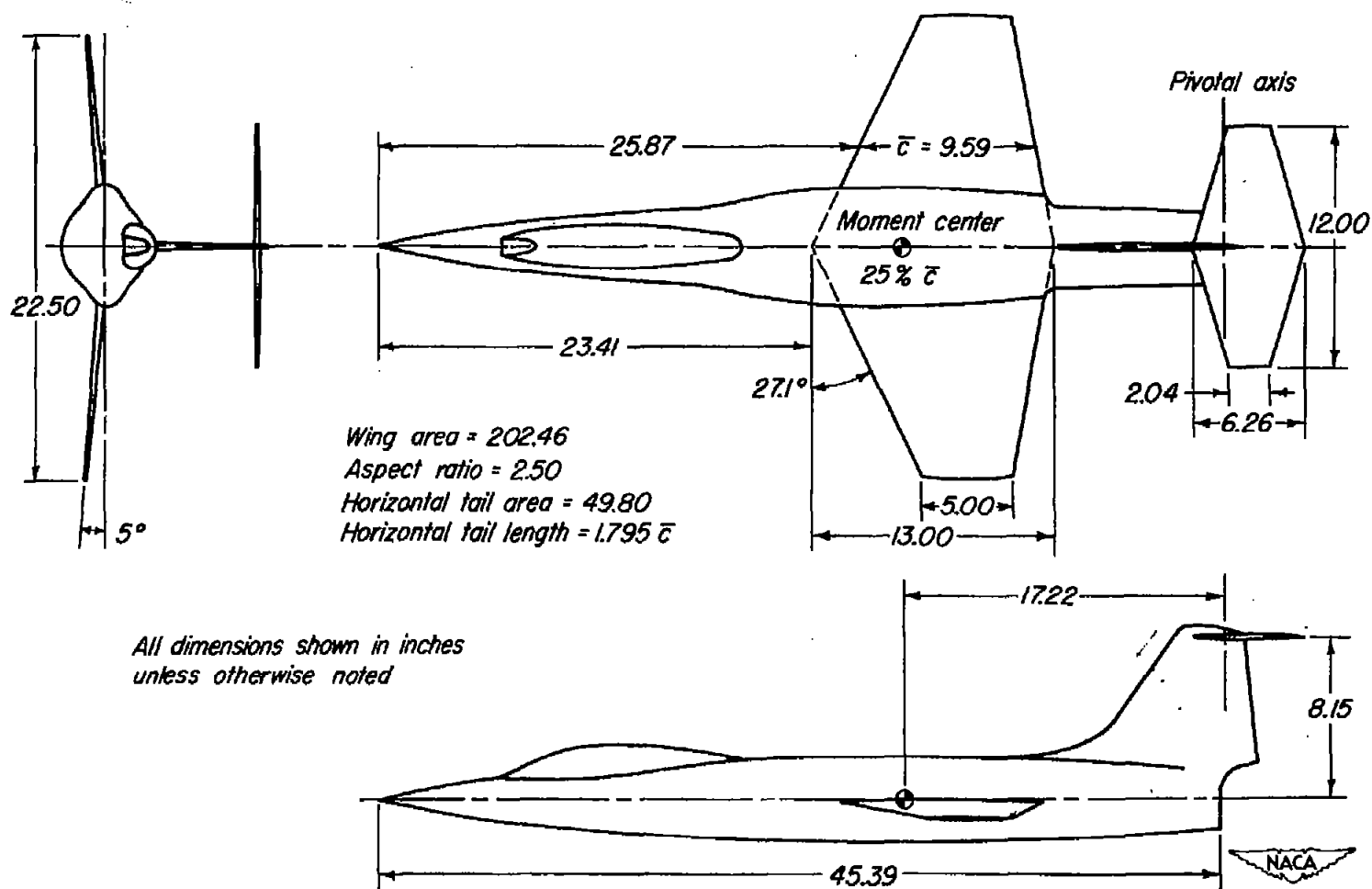


Figure 2.- Dimensional sketch of the model.

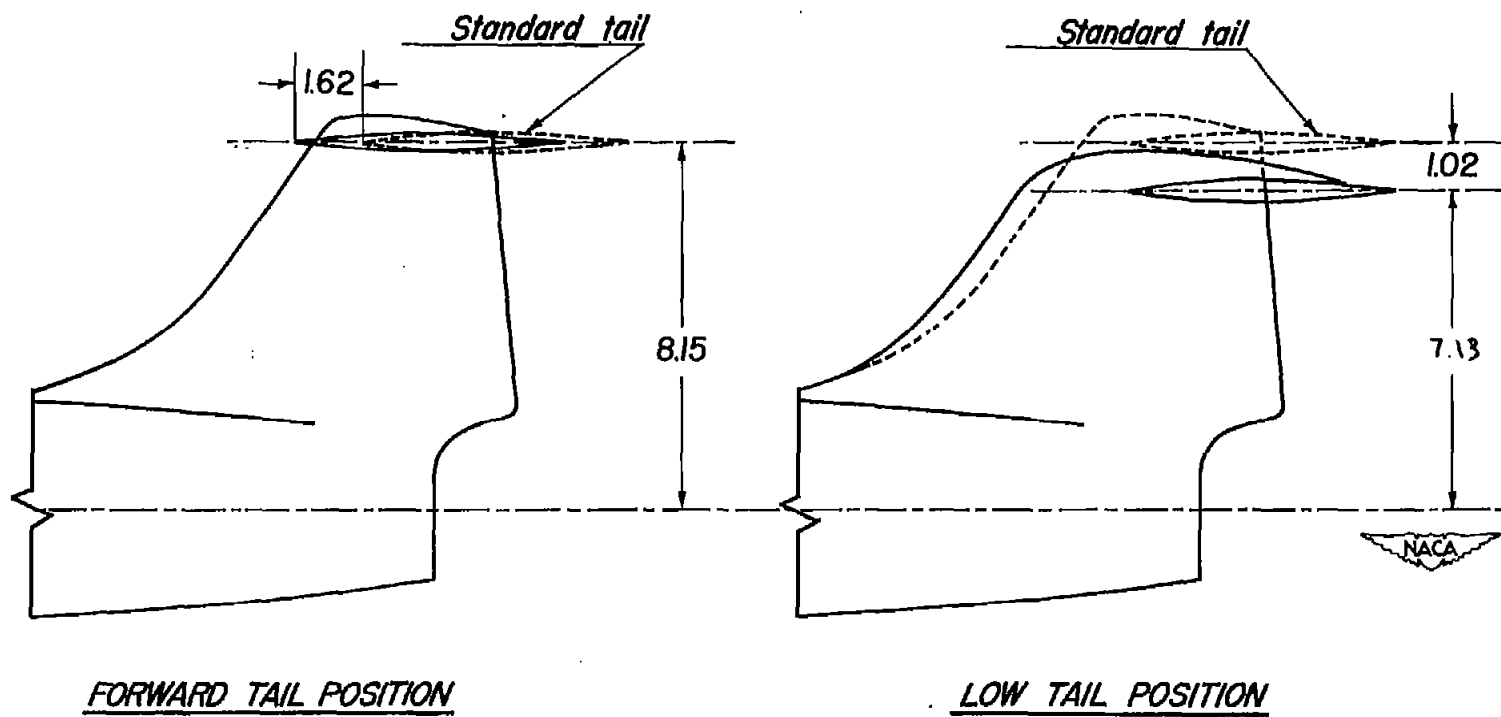


Figure 3.- Comparison of the three tail configurations.

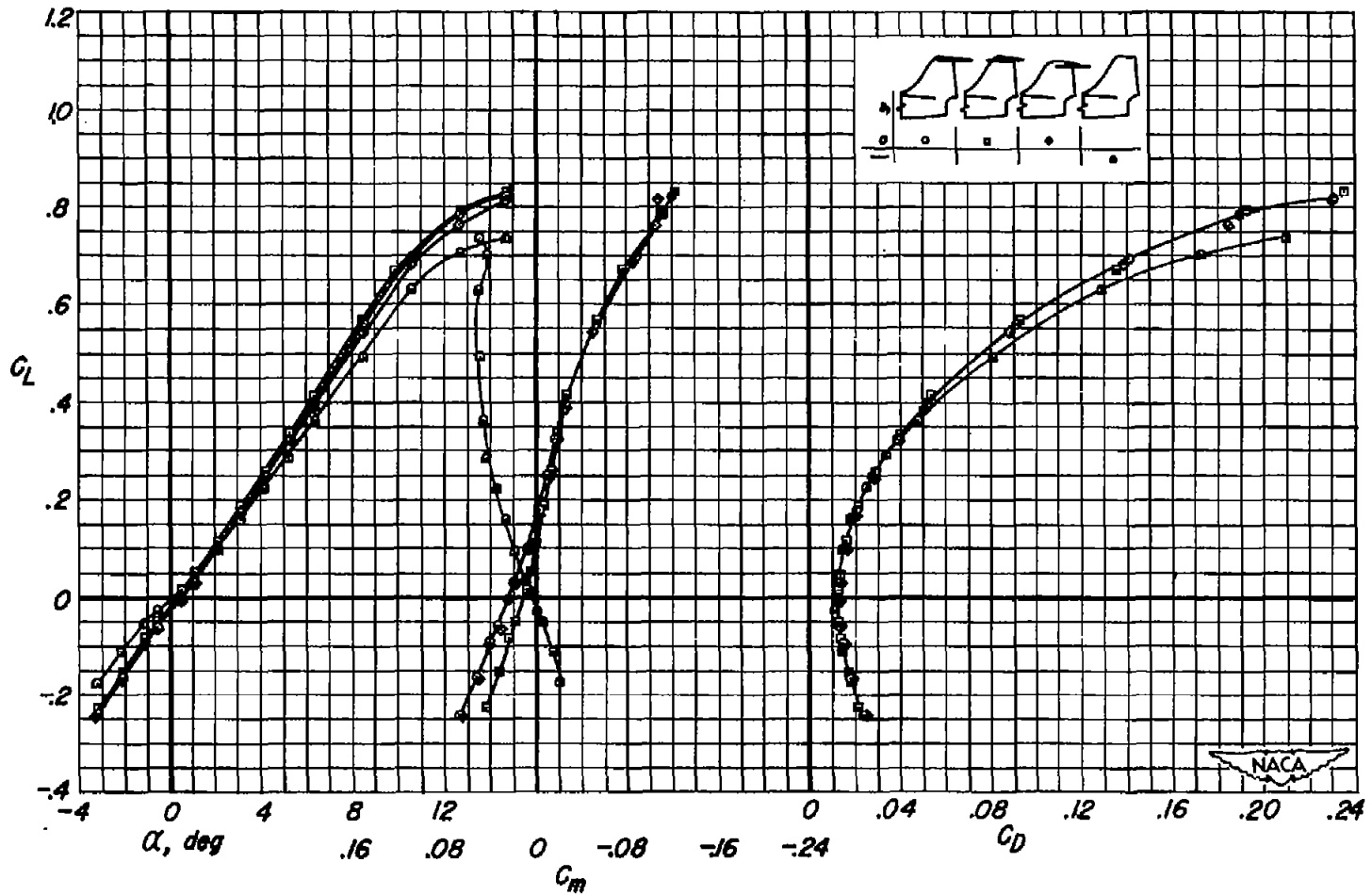
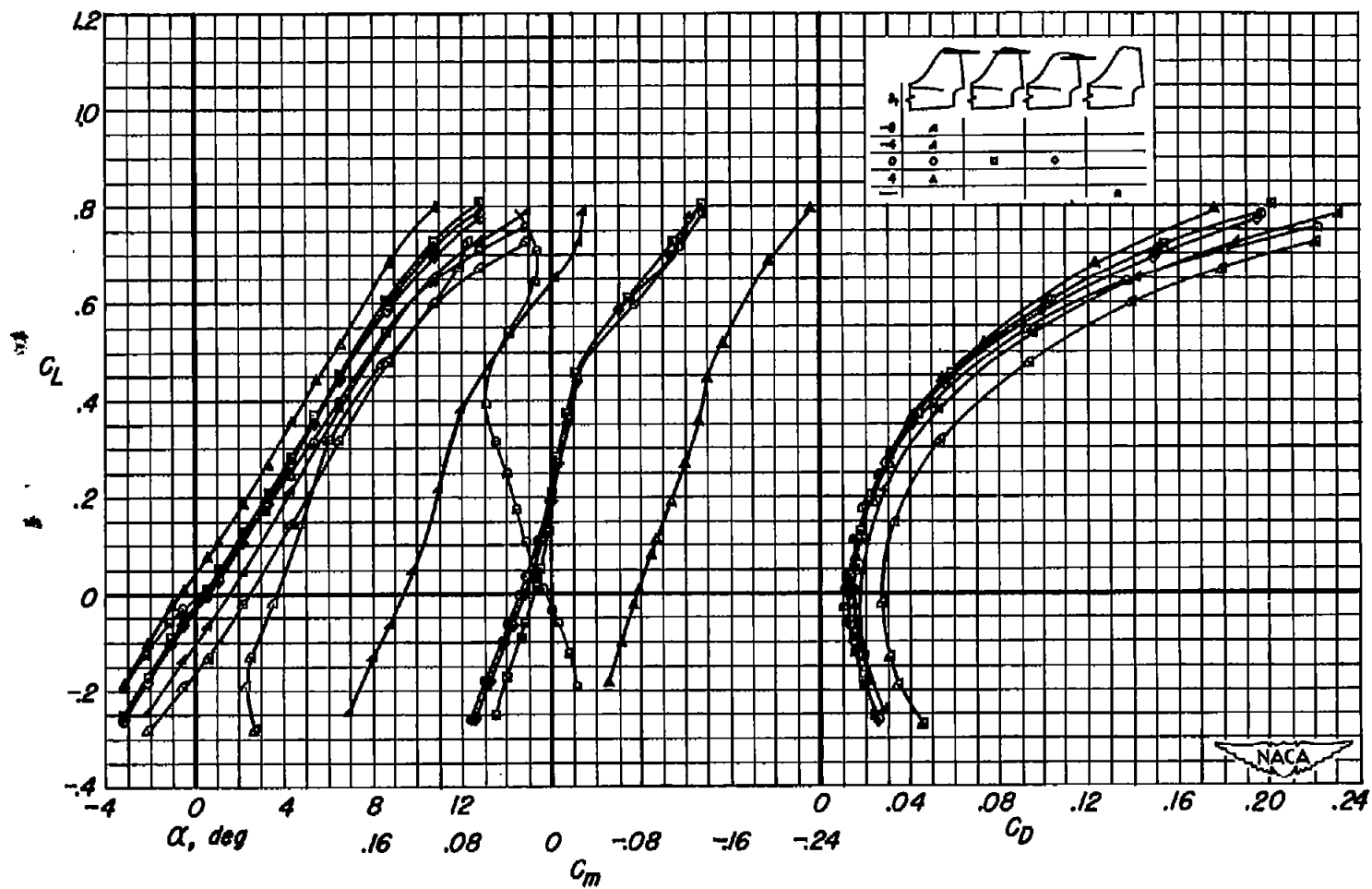
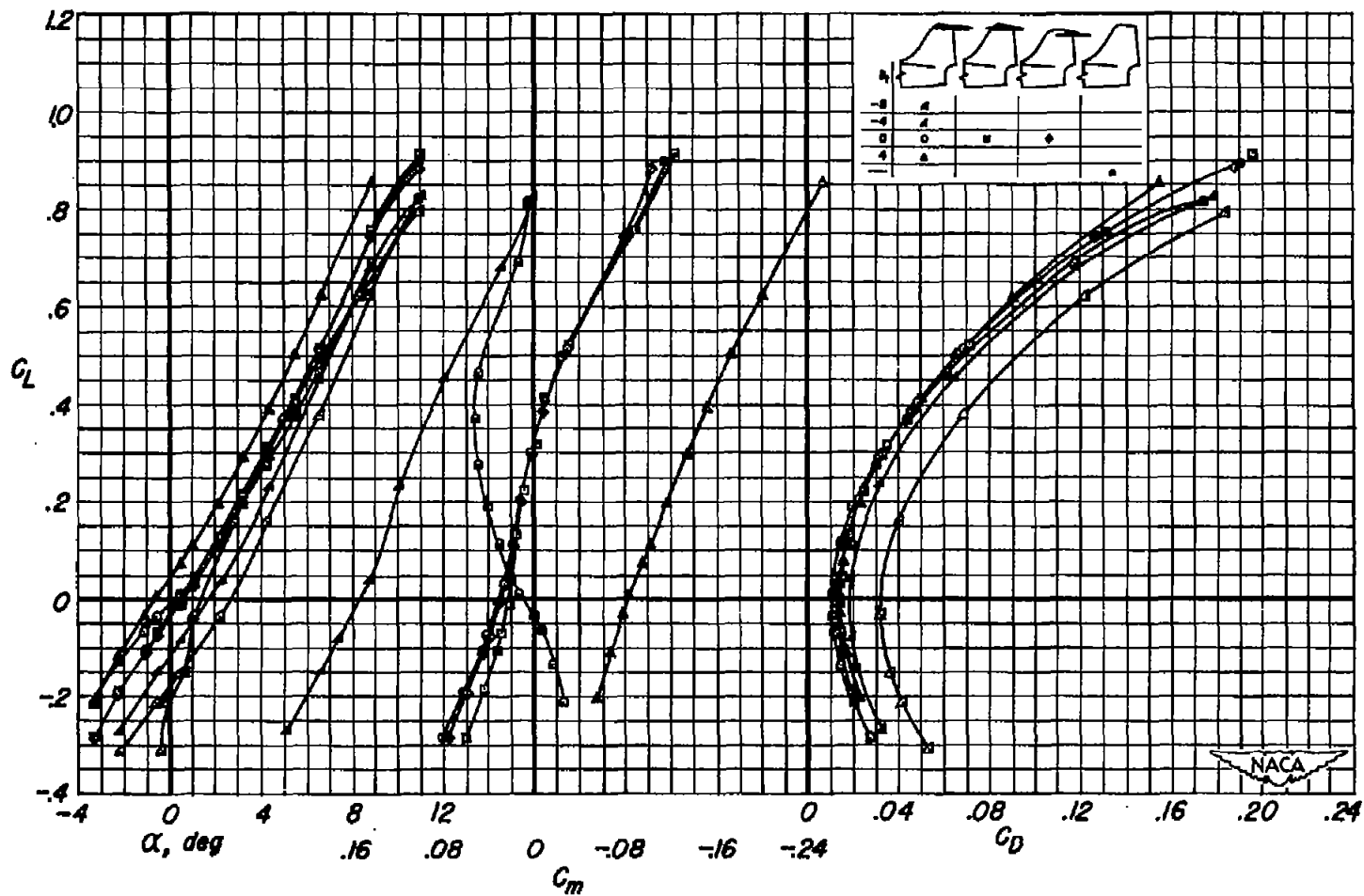
(a) $M = 0.60$

Figure 4.- Variation of angle of attack and pitching-moment and drag coefficients with lift coefficient.



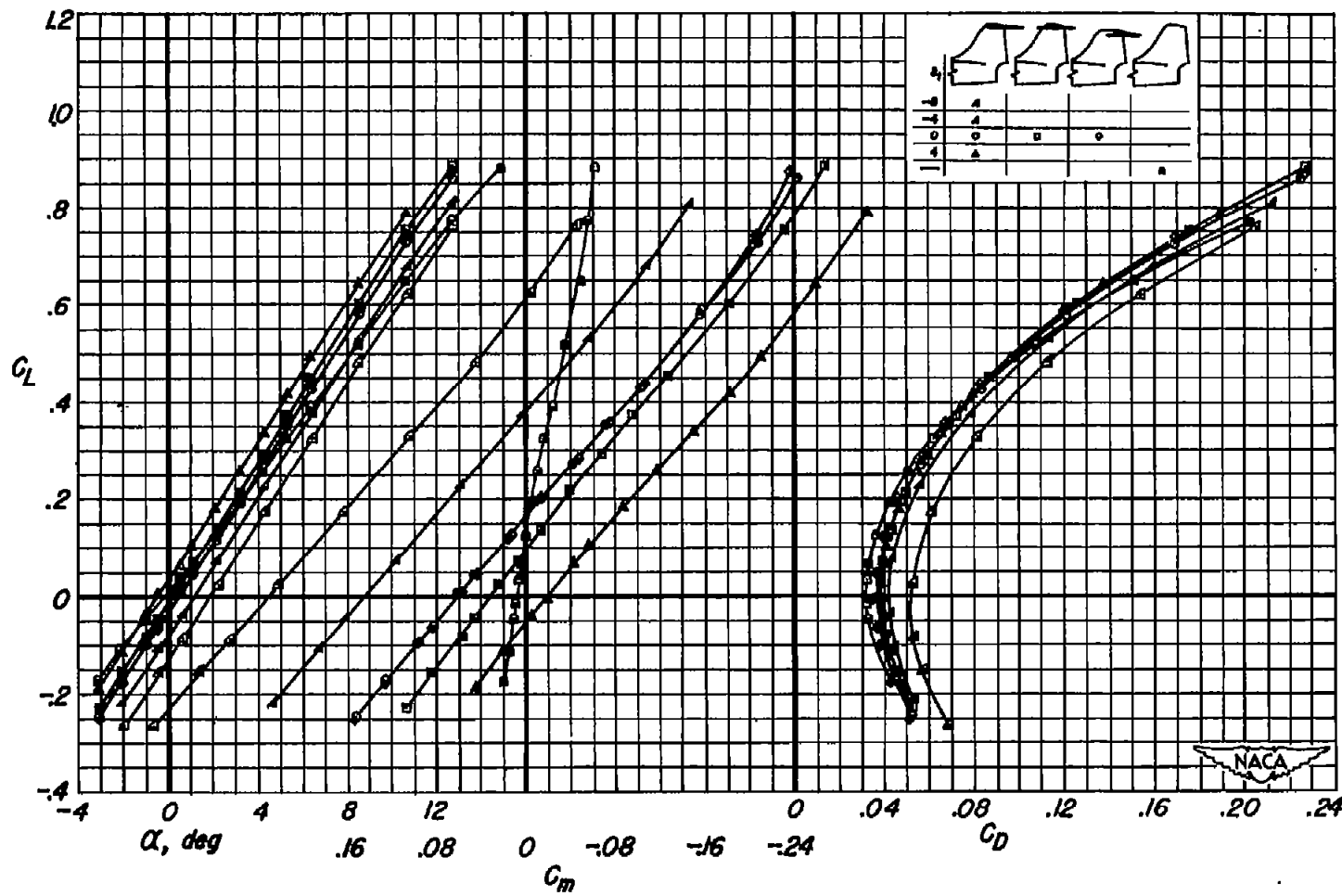
(b) $M = 0.80$

Figure 4.- Continued.



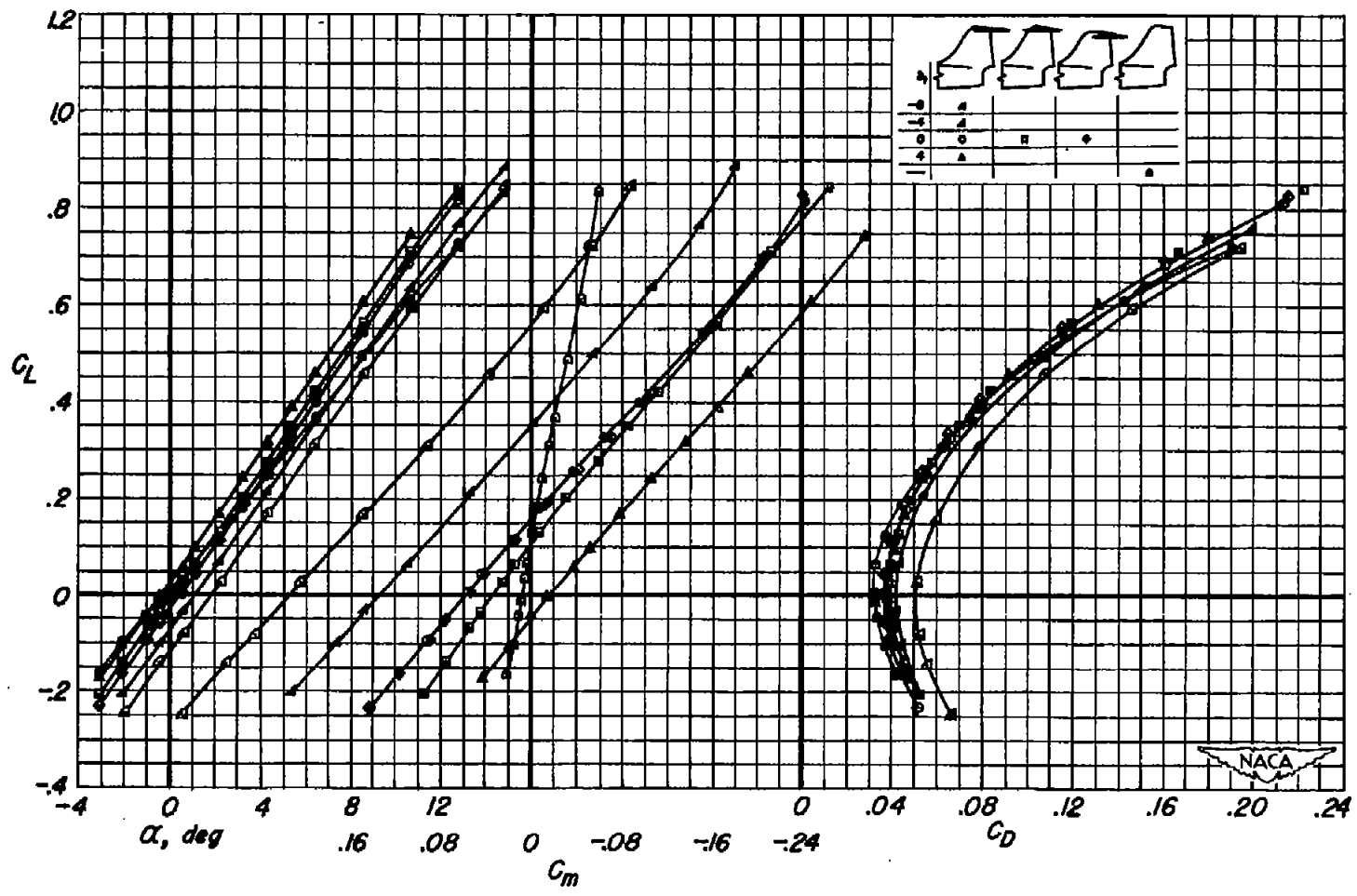
(c) $M = 0.90$

Figure 4.- Continued.



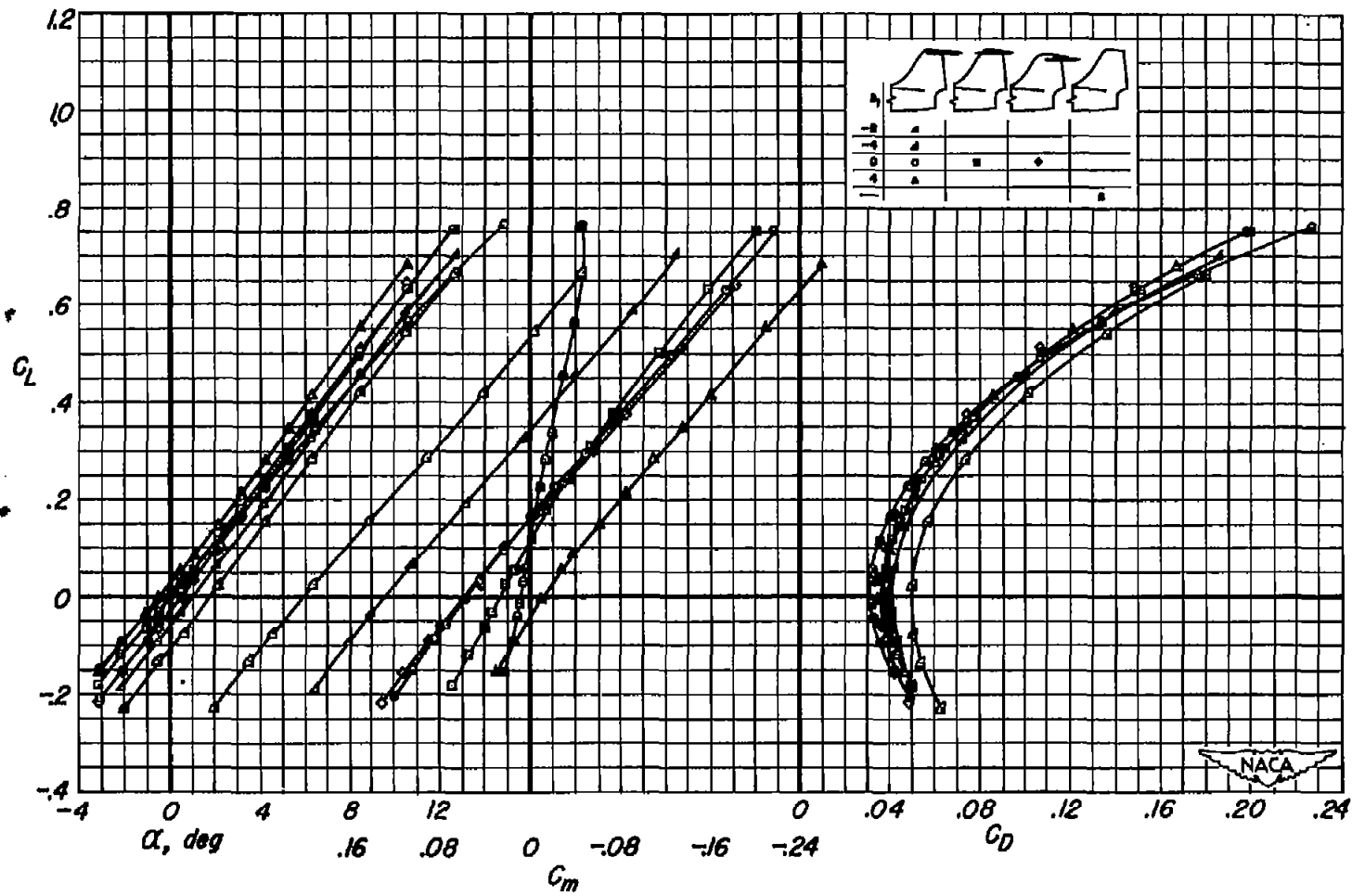
(d) M = 1.35

Figure 4.- Continued.



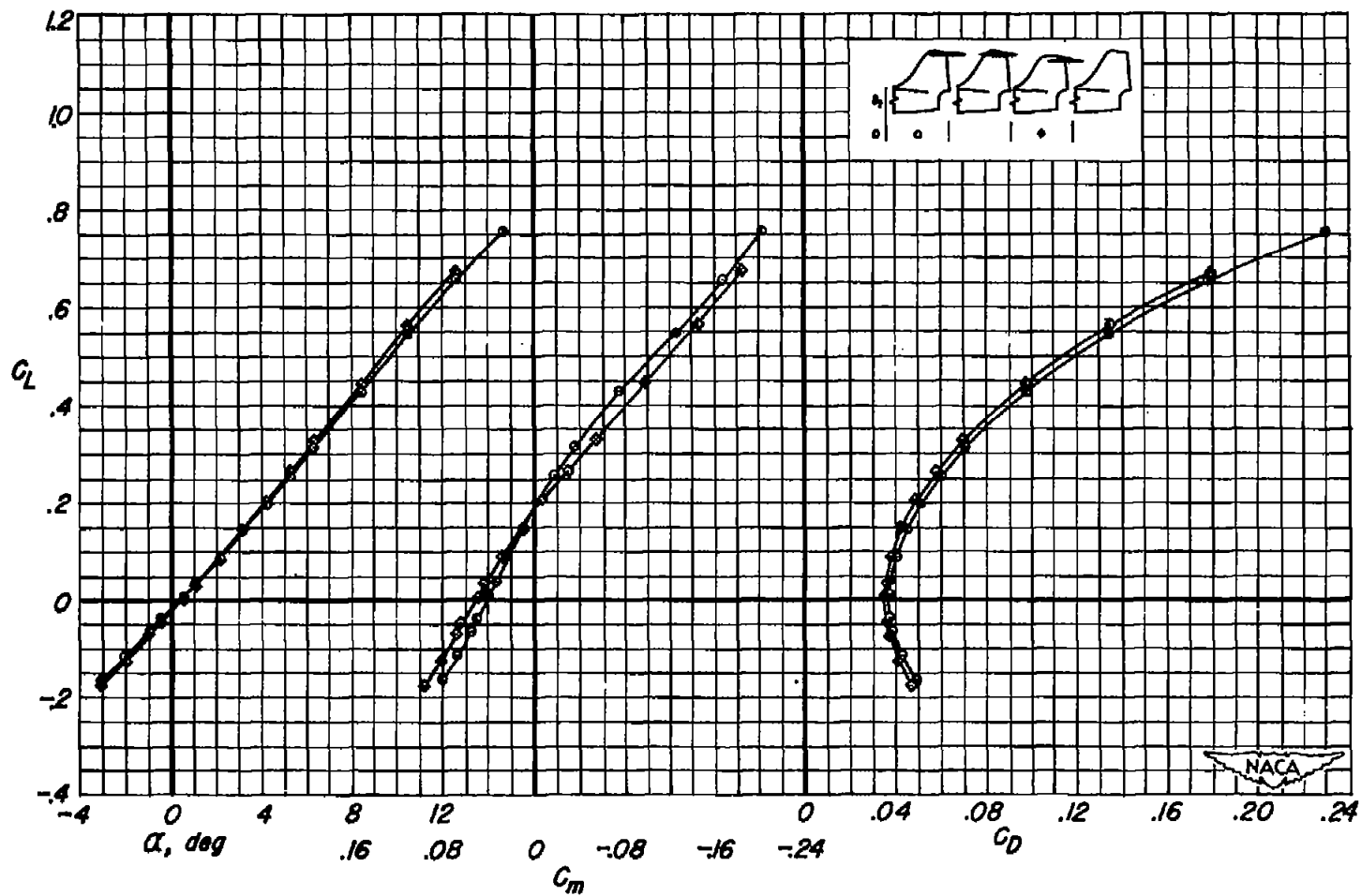
(e) $M = 1.45$

Figure 4.- Continued.



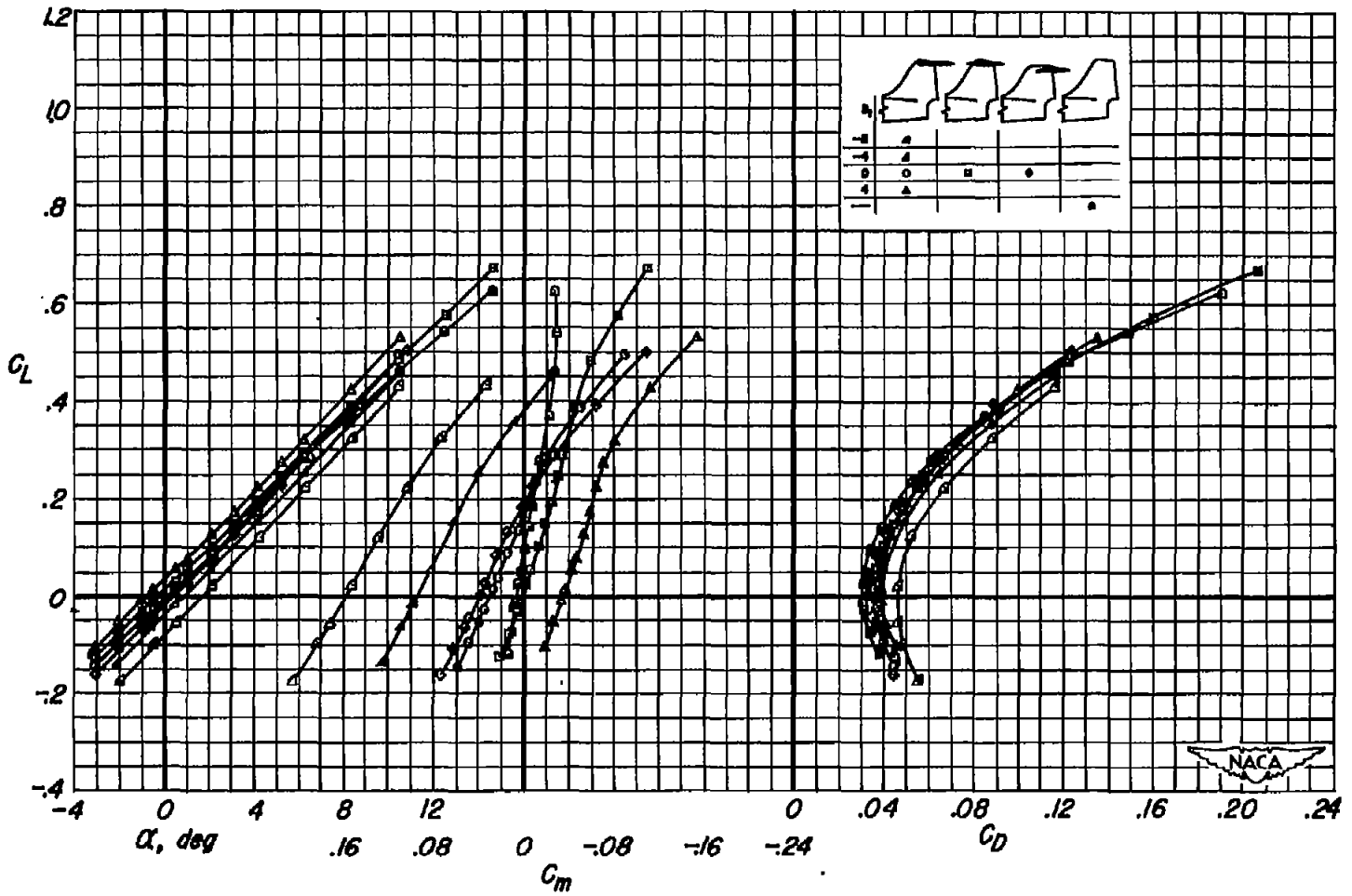
(f) $M = 1.60$

Figure 4.- Continued.



(g) $M = 1.80$

Figure 4.- Continued.



(h) $M = 1.90$

Figure 4. - Concluded.

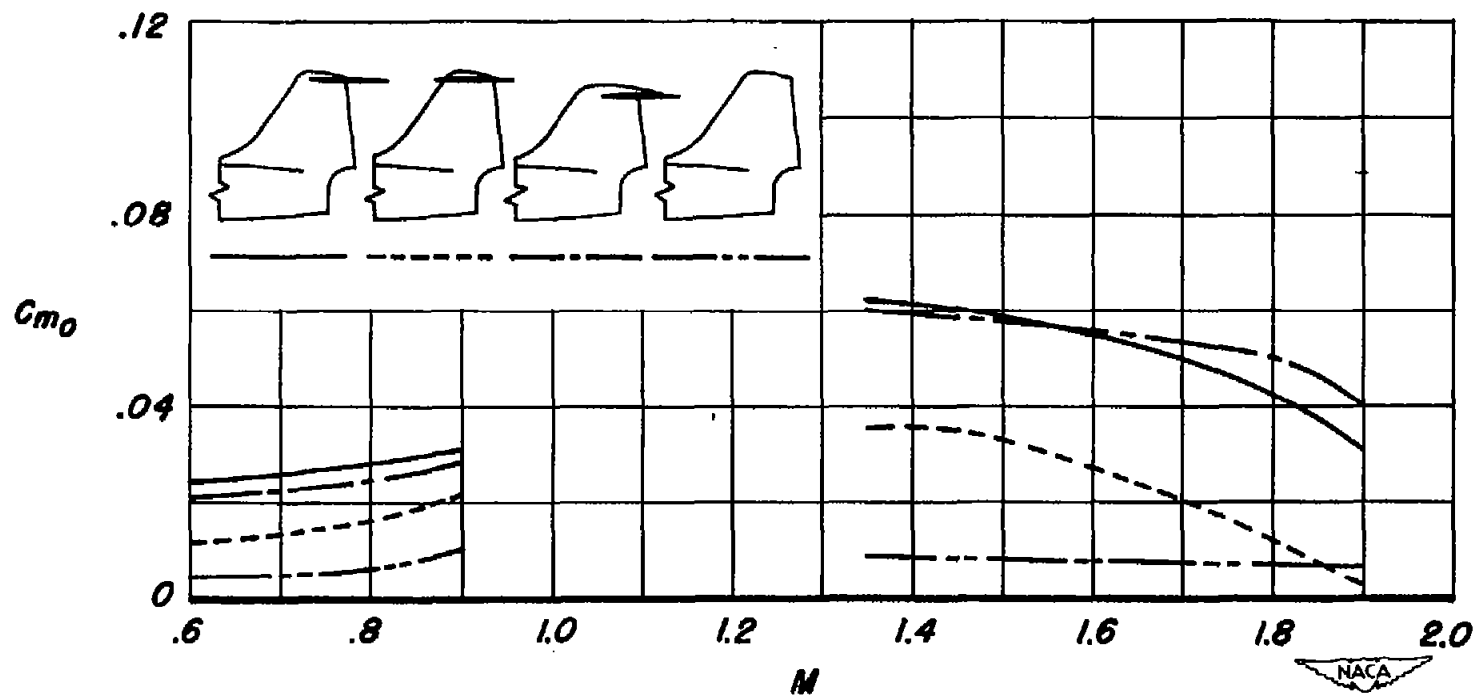
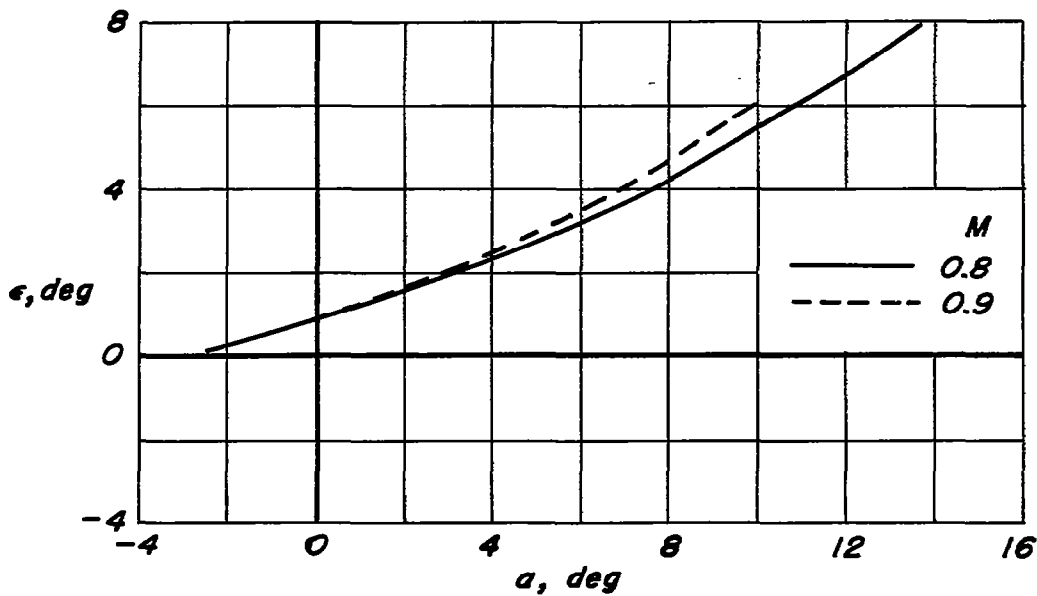
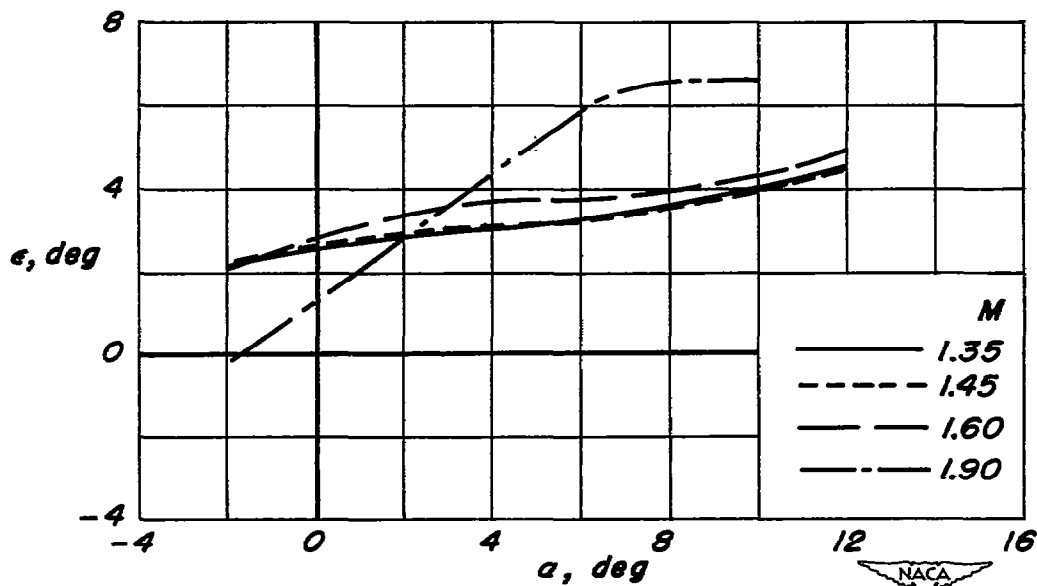


Figure 5.- Variation of pitching moment at zero lift for several tail configurations.



(a) $M < 1.0$



(b) $M > 1.0$

Figure 6.- Variation of downwash angle with angle of attack (obtained with the standard tail).

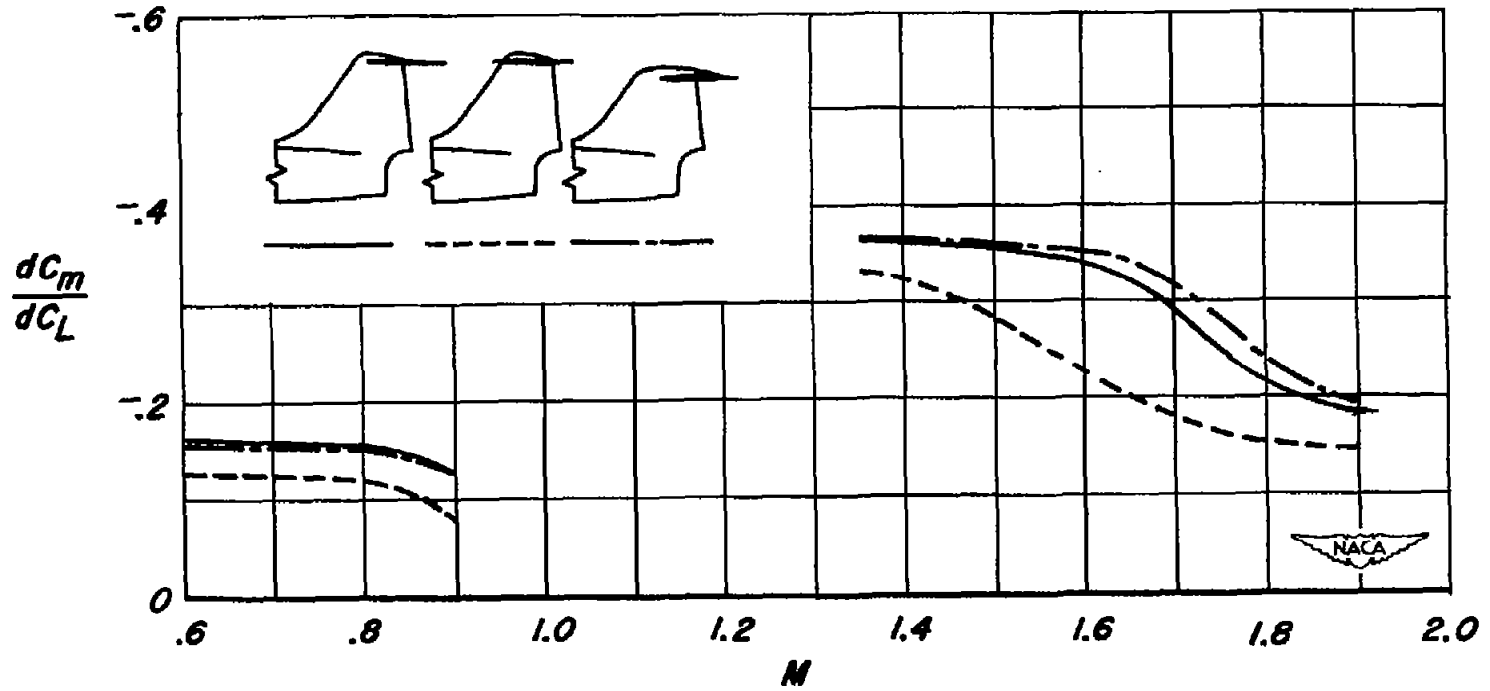


Figure 7.- Variation of stability with Mach number for the model with three tail configurations.

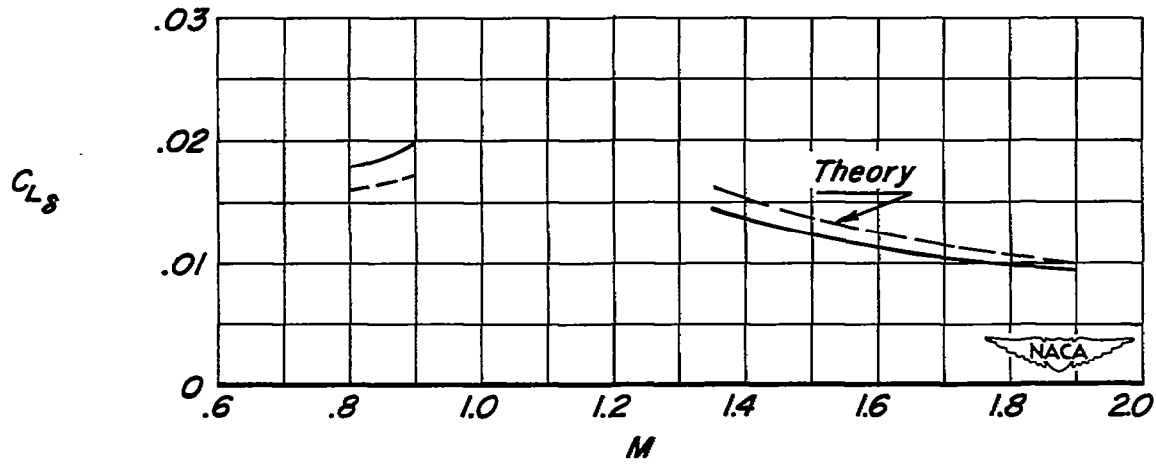
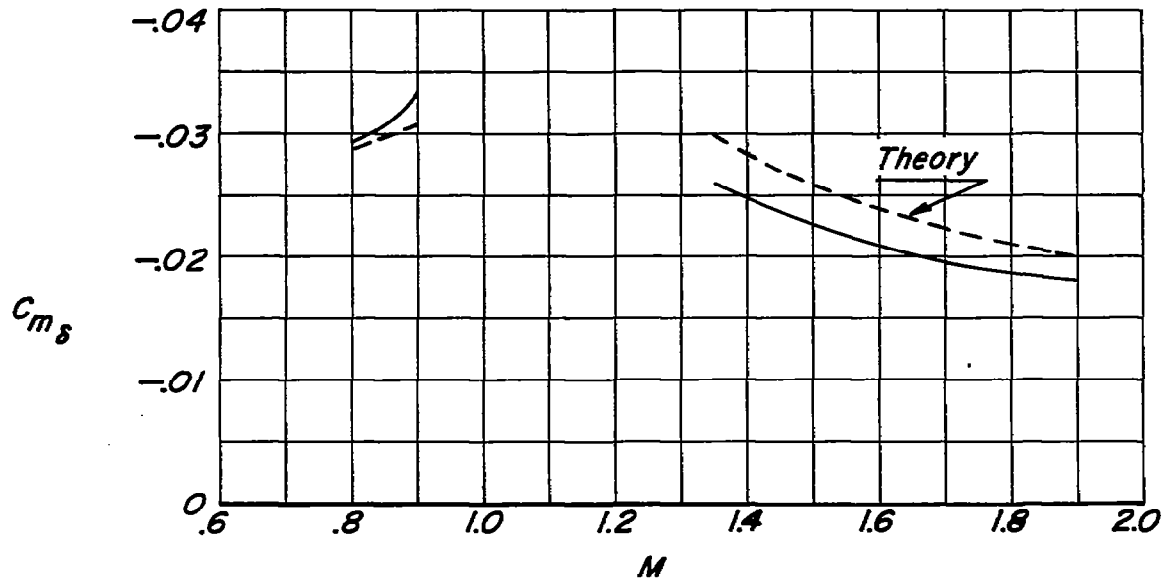


Figure 8.- Variation of tail effectiveness with Mach number; standard tail.

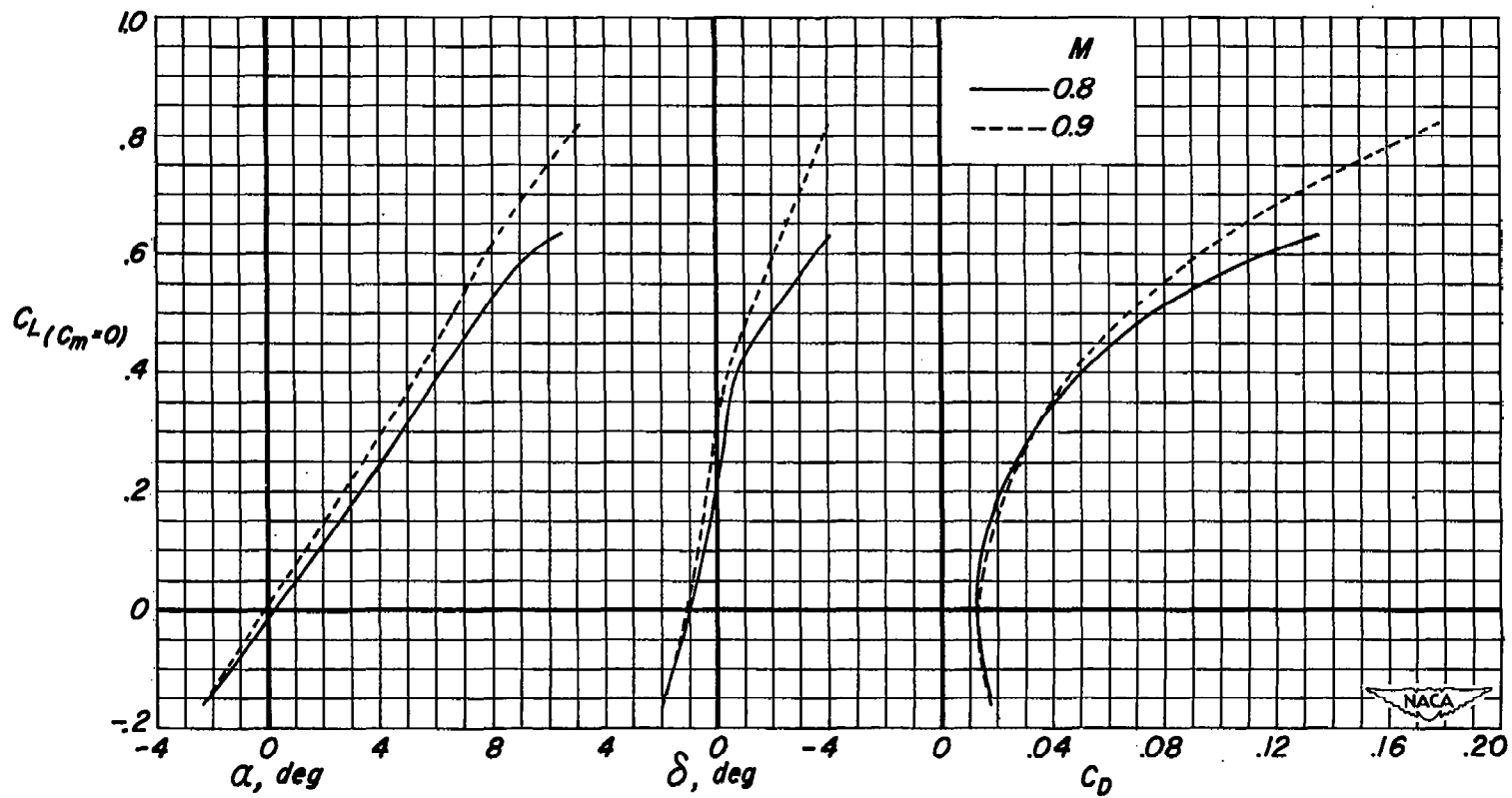
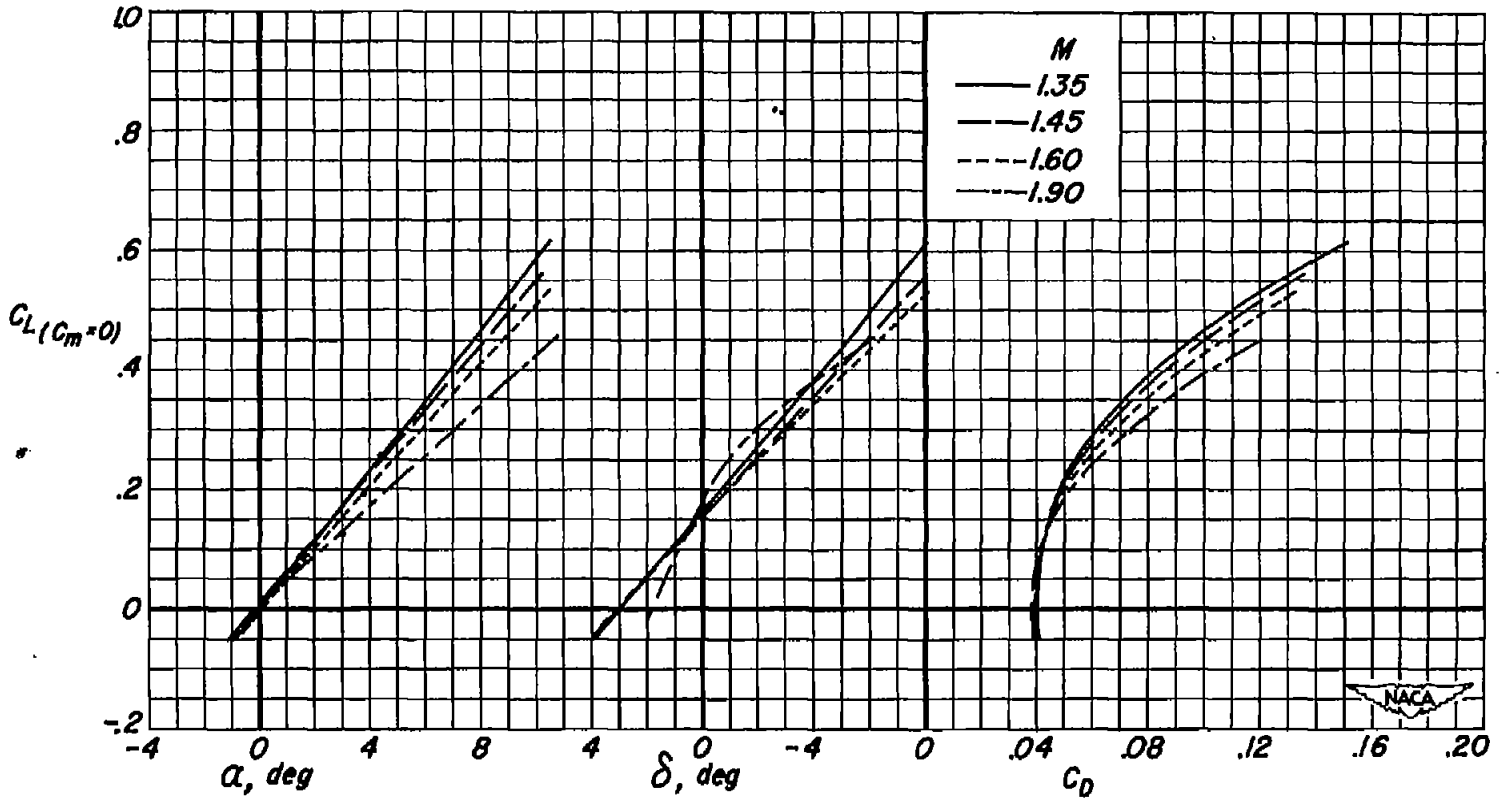
(a) $M < 1.0$

Figure 9.- Relationship of angle of attack, control deflection angle, and drag coefficient to lift coefficient for the model longitudinally balanced with the standard tail.



(b) $M > 1.0$

Figure 9.- Concluded.

$M/S = 5.0$
 $n = 60,000'$